Theoretical investigation of charge density wave instability in CuS_2

Yuxin Yin,[1,2] Jennifer Coulter,[1] Christopher J. Ciccarino,[1,3] and Prineha Narang[1,*]

[1]*John A. Paulson School of Engineering and Applied Sciences, Harvard University, Cambridge, 02138 Massachusetts, USA*

[2]*Department of Materials, University of Oxford, Oxford, OX1 4BH Oxfordshire, United Kingdom*

[3]*Department of Chemistry and Chemical Biology, Harvard University, Cambridge, 02138 Massachusetts, USA*

(Received 24 September 2019; revised 28 April 2020; accepted 1 September 2020; published 2 October 2020)

The existence of a charge density wave (CDW) in transition-metal dichalcogenide (TMDC) CuS_2 has remained undetermined since its first experimental synthesis nearly 50 years ago. Despite conflicting experimental literature regarding its low-temperature structure, there exists no theoretical investigation of the phonon properties and lattice stability of this material. By studying the first-principles electronic structure and phonon properties of CuS_2 at various electronic temperatures, we identify temperature-sensitive soft phonon modes which unveil a previously unreported Kohn anomaly at approximately 100 K. Variation of the electronic temperature shows the presence of two distinct phases, characterized at low electronic temperature by a $2 \times 2 \times 2$ periodic charge modulation associated with the motion of the S_2 dimers. We find this is driven by a slight orbital occupation imbalance of the copper d and sulfur p orbitals, reminiscent of the Jahn-Teller effect in finite systems. Investigation of the Fermi surface presents a potential Fermi surface nesting vector related to the location of the Kohn anomaly and observed band splittings in the unfolded band structure. The combination of these results suggests a strong possibility of CDW order in CuS_2. Further study of CuS_2 in monolayer form finds no evidence of a CDW phase, as the identified bulk periodic distortions cannot be realized in two dimensions. This behavior sets this material apart from other transition-metal dichalcogenide materials, which exhibit a charge density wave phase down to the two-dimensional limit. As CDW in TMDC materials is considered to compete with superconductivity, the lack of a CDW in monolayer CuS_2 suggests the possibility of enhanced superconductivity relative to other transition-metal dichalcogenides. Overall, our work identifies CuS_2 as a previously unrealized candidate to study the interplay of superconductivity, CDW order, and dimensionality.

DOI: 10.1103/PhysRevMaterials.4.104001

I. INTRODUCTION

Transition-metal dichalcogenides (TMDCs) such as Ta, $Nb(S,Se)_2$ have displayed interesting physics including charge density wave (CDW) formation and low-temperature superconductivity [1–7]. While bulk, layered TMDC structures can host CDWs, recent studies have investigated the competition between CDW order and superconductivity [7–9], as well as the enhancement of superconducting T_c in monolayer TMDCs in relation to the suppression or lack of CDW order [10–15]. Despite the lack of a unified understanding of the origins of CDW in TMDCs, thus far, studied examples have displayed similar CDW characteristics down to the two-dimensional (2D) limit, possibly limiting T_c enhancement.

Though the superconducting behavior of TMDC CuS_2 is well known [16], there exists a long-standing debate about the existence of CDW order in this material [17,18]. Initial studies of bulk susceptibility [16,19], nuclear magnetic resonance [17,19,20], and specific heat [17,20] have presented evidence of a second-order structural phase transition at 150 K, hinting at the formation of a CDW structure. However, a more recent experiment rejected this possibility as a result of a contradictory Hall coefficient measurement [18], and this stance has been adopted by subsequent studies.

Throughout this experimental debate, theoretical study of CuS_2 has remained extremely limited [21–23]. Presently, there are no reports of the phonon properties of CuS_2, which could provide critical insight regarding its structural phases. Theoretical studies of other CDW materials, including $NbSe_2$ [24], $TiSe_2$ [25,26], and $TaSe_2$ [27], have successfully captured CDW behavior and related phenomena through analysis of electronic-temperature-dependent structural and electronic properties.

In this context, we present *ab initio* calculations of the electronic and phononic properties of CuS_2 as a function of electronic temperature [28,29], which is modeled using the Fermi-Dirac smearing width. We observe that the experimentally reported high-temperature structure [16] exhibits instabilities and a Kohn anomaly in the phonon dispersion for calculations at low T_e. By constructing and stabilizing a superstructure of CuS_2, we report the existence of a $2 \times 2 \times 2$ periodic manifestation of this material. We find that the transition to the distorted structure is governed by a twice-periodic displacement of the S_2 dimers of CuS_2, related to opposite breathing modes of the Cu octahedra. This results in a modulation of the charge density of the same periodicity. We find this phenomenon is caused by an unequal occupation of copper d and sulfur p orbitals, which drives the system into lower symmetry, reminiscent of a Jahn-Teller effect. By evaluating the electronic structure of the low-temperature distorted structure, we observe the appearance of band splittings and identify

*prineha@seas.harvard.edu

a potential Fermi surface nesting vector associated with the Kohn anomaly. Subsequently, we investigate monolayer CuS_2 [30] and find no instabilities or any other hints of CDW formation, regardless of electronic temperature, possibly because it cannot host the dimer motions observed in the bulk structural distortion.

Together, our results strongly suggest CDW order in bulk CuS_2 and, by identifying its origins, explain the absence of CDW in the 2D limit. We therefore present it as an exemplary platform to study the competition between superconductivity and CDW order and, in particular, the role dimensionality plays in these effects. We discuss the unique aspects of CDW formation relative to well-known TMDC materials, and further discuss pathways for enhancing superconductivity in both bulk and monolayer CuS_2.

In textbook one-dimensional (1D) systems, the origin of CDW is conventionally analyzed in the Peierls instability picture [31–33], where the system undergoes a periodic lattice distortion characterized by charge density modulation to form a symmetry-reduced state. This results in band splittings at the Fermi wave vector ($\vec{k}_F$) related to a Fermi surface nesting vector $\vec{k}_{\text{nesting}} = 2\vec{k}_F$, which connects multiple points on the Fermi surface and indicates the location of a Kohn anomaly in the phonon dispersion [34]. However, in higher-dimensional systems, the analogy to the Peierls instability is not as straightforward [35] and Fermi surface nesting alone is generally not sufficient for understanding the origin of CDW formation. Other mechanisms include the excitonic insulator instability [26,36], Jahn-Teller effects [36], and momentum-dependent electron-phonon coupling [24,35,37], as well as a combination of these mechanisms.

II. METHODS

Therefore, to investigate the occurrence of CDW in CuS_2, we begin by considering its structural stability. We start with the experimental pyrite ($Pa3$) structure measured at ambient temperatures [16,17], with Cu atoms occupying fcc sites of the unit cell, and S_2 dimers centered along cell edges. We note this pyrite structure adopted by CuS_2 is quite distinct from other layered TMDCs such as NbS_2 which have spatially separated layers interacting by weak van der Waals forces. After structural relaxation, we perform density functional theory (DFT) [38] calculations with computational procedures previously introduced [39–42]. To describe CuS_2, we selected the ultrasoft Rappe Rabe Kaxiras Joannopolous pseudopotentials [43,44] parameterized for the Perdew-Burke-Ernzerhof exchange-correlation functional [45]. We also include a Hubbard U parameter (DFT + U) of $U_{\text{eff}} = 0.5$ eV, as determined from first-principles linear response [46]. This relatively small U_{eff} is consistent with experimental studies which have found weak electronic correlation [18,23] in CuS_2, as we find the bands near the Fermi energy are mostly of sulfur p (as opposed to copper d) character. Calculations analyzing the impact of U on results are shown in the Supplemental Material [47].

The density functional theory electronic structure and phonon calculations performed were all converged using a 20-Hartree plane-wave energy cutoff for the kinetic energy and an 80-Hartree cutoff for the charge density. We have also performed calculations at a 40-Hartree kinetic energy cutoff (with corresponding 160-Hartree charge density cutoff) and find no appreciable changes in our results. We used a $6 \times 6 \times 6$ k-point mesh and a $2 \times 2 \times 2$ phonon supercell to model the electronic and phononic properties of the 12-atom unit cell. We used equivalent wave-vector sampling densities when modeling the distorted $2 \times 2 \times 2$ superstructure (i.e., a $3 \times 3 \times 3$ k-point mesh and a $1 \times 1 \times 1$ phonon supercell). Finally, for the monolayer structure, we used a $6 \times 6 \times 1$ k-point mesh and a $2 \times 2 \times 1$ phonon supercell.

In order to probe temperature-dependent phenomena in CuS_2, we use the Fermi-Dirac smearing scheme to mimic an electronic temperature. Throughout this paper we label electronic temperature by T_e and note it is distinct from the lattice temperature. All calculations where the smearing width or electronic temperature is not specified use a 0.001 Hartree smearing (equivalent to $T_e = 315$ K). We compare our results using Fermi-Dirac smearing with other smearing methods in the Supplemental Material (SM) [48]. Finally, to compare the electronic structure of low- and high-symmetry structures, we apply a band-unfolding technique. Here we determine the overlap of the supercell Bloch states with those of the primitive cell using a symmetry-averaged spectral function technique [49], as outlined in Ref. [50].

III. RESULTS AND DISCUSSION

A. Bulk

Initial calculations of the phonon dispersion of the experimental, high-temperature structure using low-T_e smearing reveal four soft phonon modes at the R point shown in Fig. 1(a). Upon varying the smearing parameter, we found these soft modes near this wave vector to be strongly sensitive to T_e, as shown in Figs. 1(b) and 1(c). We note the appearance of a discontinuity in the phonon dispersion (a Kohn anomaly) located at wave vector $\vec{q} = \vec{R}$ for an electronic temperature corresponding to approximately 100 K.

Motivated by past experimental work suggesting the existence of a $2 \times 2 \times 2$ superstructure in CuS_2 at low temperatures [51], we sought to resolve the structural instability by using a $2 \times 2 \times 2$ supercell. The predicted phonon dispersion of the constructed supercell reveals four negative phonon modes at an electronic temperature of 32 K, consistent with the instabilities observed in the unit cell structure. We note the soft modes observed are at the Γ point of the supercell, which is equivalent to the R point in the original cell due to the corresponding change in the Brillouin zone of the supercell structure (see Fig. S1 in the SM [47]).

We identify the atomic displacements resulting from the four unstable phonon modes and observe each mode corresponds to $2 \times 2 \times 2$ periodic sideways motions of S_2 dimers, which cannot be captured in the single unit cell. These four modes collectively manifest themselves as an effective motion of the S_2 dimers with a period of $2a$, twice the original unit cell lattice coefficient, as schematically shown in Fig. 2(e).

We perform energy minimization with respect to the ground-state energy of the high-symmetry phase as a function of the magnitude of the eigendisplacements of each of these modes (for illustration of the individual modes and energy

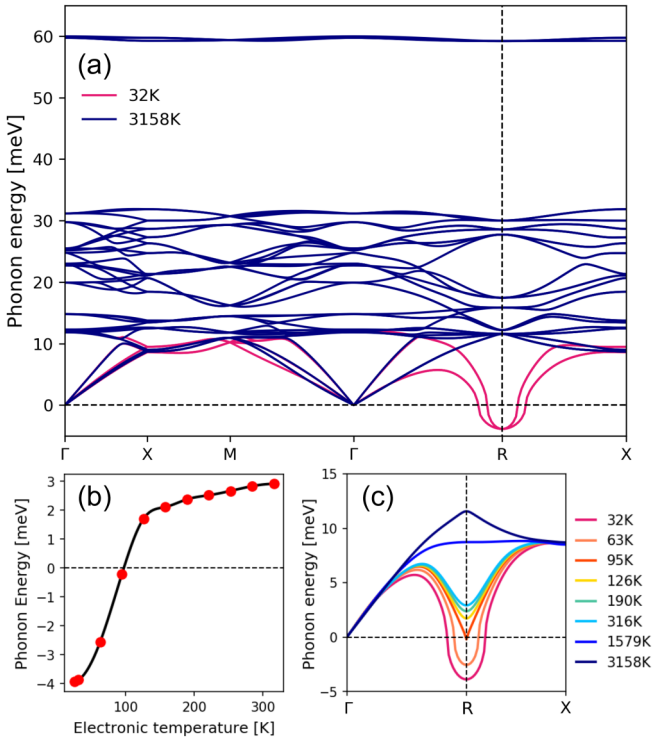

FIG. 1. Structural stability of CuS_2. (a) The predicted phonon dispersion for the CuS_2 unit cell experimentally established in high temperature measurements [16] when calculated for low and high electronic temperatures. (b) The lowest phonon frequency as a function of electronic temperature, and (c) a close-up of the instability showing its temperature dependence and the Kohn anomaly observed near 100 K. From these calculations, we uncover a key difference between the low- and high-temperature structures of CuS_2 which indicates the existence of a structural phase transition.

minimization, see Fig. S2 in the SM [47]). By applying this collective distortion to the constructed undistorted superstructure, we obtain a distorted structure with reduced symmetry, from $Pa3$ to P-1 as shown in Fig. 2(d), and predict a stable phonon dispersion at low T_e. By comparing the undistorted and distorted structures and calculating the difference in their charge densities, we identify a $2a$ periodic modulation of charge density, commensurate with the periodicity of the distorted structure, as shown in Fig. 2(f).

Additionally, we investigate the relative stability of the undistorted and distorted supercells [Fig. 2(b)], and find that as we change the electronic temperature of both structures, we see a crossover in the ground-state energy at about 150 K, a transition that would agree impressively well with experimental results [17] and correspond to what was calculated in Figs. 1(b) and 1(c). When relaxed at higher T_e, the distorted structure returns to the undistorted structure, indicating the process can be reversed.

The combination of the observed Kohn anomaly, periodic lattice distortion, periodic charge density modulation, and temperature-dependent phase crossover are all indicative of the presence of a CDW in bulk CuS_2. Our results therefore theoretically capture a stable low-electronic-temperature distorted phase of CuS_2 exhibiting strong indicators of CDW ordering.

To understand the electronic origins of the potential CDW phase, we investigate the corresponding changes in the electronic structure. We start by looking at the changes in occupation as a result of the lattice distortion. The collective distortions shown in Fig. 2(d) introduce alternating expansions and compressions of the Cu-centered octahedra. We note this kind of alternating breathing has been observed in the context of other types of transitions, including site-selective Mott metal-insulator transitions in $ReNiO_3$ [52]. We find that these alternating motions introduce crystal field splitting and shift the orbital occupations of both the Cu d and sulfur p orbitals.

Figure 3(a) shows the typical energy level diagram for octahedra complexes, where the e_g-type d orbitals are degenerate but higher in energy than degenerate t_{2g}-type d orbitals, in addition to the alternating expansion and compression modes we find. We analyzed the total occupations of each of these orbitals by evaluating the orbital-projected density of states. In Fig. 3(d), we plot the resulting occupations for each of the copper d and sulfur p orbitals in the $2 \times 2 \times 2$ supercell, with the x axis corresponding to arbitrary labeling of each atomic species. Interestingly, we find that in the distorted structure, a general trend is observed where there are alternating occupation preferences between the different Cu e_g, Cu t_{2g}, and S p orbitals. This is distinct from the undistorted case, where the occupations are fixed and do not alternate. Figure 3(c) shows the arrangement of the e_g occupation preference in the distorted phase, where we can see alternating occupation preference. The distortions allow for these alternating occupation preferences to manifest, similar to a Jahn-Teller effect in moleculelike systems. We also note that the arrangement of the orbital preference in Fig. 3(c) matches the periodicity of the sulfur dimer motion shown in Fig. 2(e), reminiscent of a "bond density wave" where chains of atoms can introduce changes in bonding in insulating crystals such as bulk Te [53]. In Fig. 3(b) we plot the total energy of the system along the 1D configuration coordinate of the alternating compression and expansion distortion, which shows dips on either side of the high-symmetry point as one would expect from a Jahn-Teller-like behavior. Altogether, we find that the orbital occupations and the total energy of the system, which are essentially electronic properties, are uniquely sensitive to this symmetry-breaking phonon mode. These are clear signatures of electron-phonon coupling. We can therefore connect the observed instability to electron-phonon interactions.

We next compare how the electronic properties of the distorted supercell are different from the undistorted unit cell. By using a band unfolding technique, we compare the effective band structure of the distorted supercell with that of the undistorted structure, seen in Fig. 4(a). We observe that the distortion results in multiple band splittings and the formation of small gaps at multiple points along the band path. The locations of these gaps tend to occur halfway between high-symmetry points (e.g., Γ and R, R and X) and slightly away from the Fermi energy level, in contrast to gap openings observed at E_F in other CDW materials [2,11,54]. In general these deviations from the overlaid high-symmetry band structures have weak spectral weights.

We note the splitting at approximately 0.2 eV above the Fermi level, which is centered at a wave vector $\vec{k}^* = \frac{1}{2}\vec{R}$, half

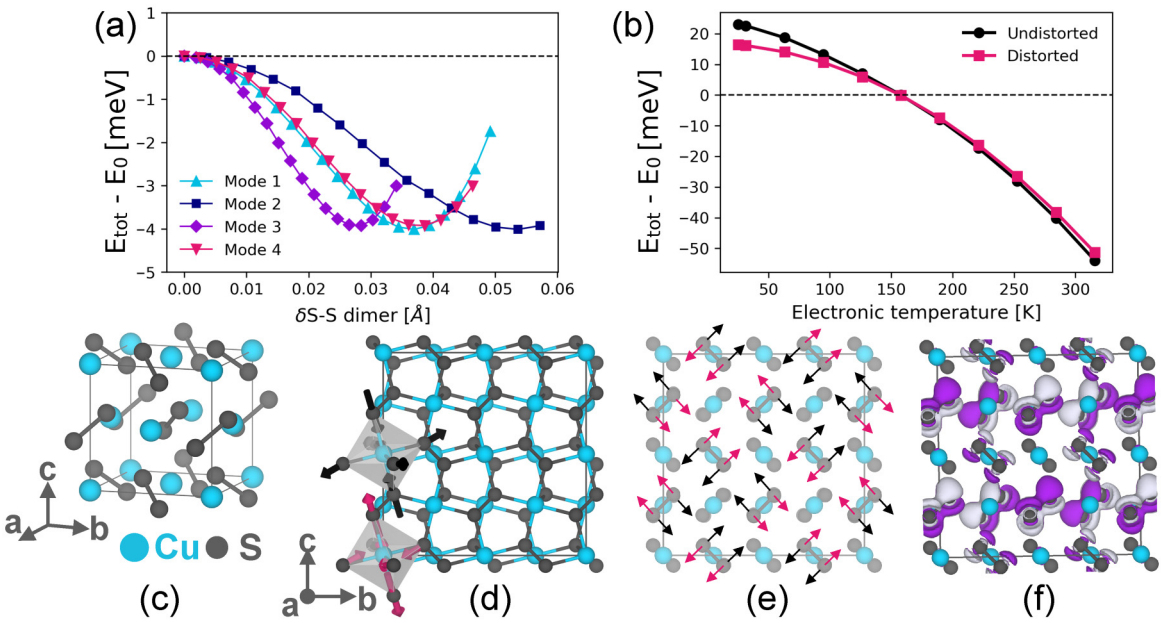

FIG. 2. Collective distortion and the appearance of CDW order in CuS_2. (a) Calculated energy (E_{tot}) relative to the energy of the undistorted $2 \times 2 \times 2$ supercell (E_0) for each of the four unstable phonon modes shown in Fig. 1. The x axis corresponds to the change in distance between neighboring sulfur atoms. The Fermi-Dirac smearing width corresponds to $T_e = 32$ K. (b) The calculated energy of the supercell in the undistorted and distorted configuration as a function of the electronic temperature (i.e., the Fermi-Dirac smearing width). The reference energy is the energy of the undistorted structure at $T_e = 150$ K. A crossover is observed around this temperature, where at lower smearing the distorted structure is lower in energy, while at higher smearing the undistorted structure is energetically favored. This is in agreement with experimental measurements [17]. (c) The high-symmetry unit cell. (d) The supercell created by a $2 \times 2 \times 2$ repeated unit cell, along with the emergent octahedra-like structural arrangement, where the Cu atom sits at the center and six sulfur atoms surround it. The arrows indicate alternating expansion and compression of the octahedra. These motions correspond to the observed effective displacement between the distorted and undistorted structures. From a different perspective, (e) shows the motion of the sulfur atoms across the supercell. (f) The result of taking the difference between the charge density of the distorted and undistorted structures, where a twice-periodic charge density oscillation is observed. The realization of this stable distorted superstructure at low electronic temperatures agrees well with early experimental reports [51], and suggests the possibility of CDW formation in CuS_2.

that of the vector where the Kohn anomaly was observed in the undistorted structure). We find that this wave vector, when overlaid with the Fermi surface (not shown), points to a saddle point in the surface, and that twice this vector ($2\vec{k}^*$) connects such saddle points diagonally across the Fermi surface. In the conventional 1D model of CDW formation [32,33], the Peierls instability results in band-gap formation at $\vec{k}_F$ and a Kohn anomaly located at $\vec{k} = 2\vec{k}_F$. These criteria appear to be met for CuS_2; however, importantly, the saddle point exists $\sim$0.2 eV above the Fermi energy. We therefore do not expect it to play a significant role in the CDW formation observed.

Additionally, we find that CuS_2 shows weak electronic correlation [55] due to the dominance of sulfur p rather than Cu d orbitals at the Fermi level, while the gaps are energetically away from the Fermi level. Figure 4(b) shows the orbital decomposed band structure of the unit cell with the relative strengths of the Cu d and S p orbitals shown along with the corresponding contributions to the density of states. The lack of strong d-orbital character at the Fermi level suggests a Mott-Hubbard-type metal-insulator transition [56] cannot provide a significant contribution to CDW formation. We also note the splitting of the d-orbital energy level as a result of compression and expansion of alternating Cu-site octahedral environments, which would account for the change in band structure approximately 0.5 eV below the Fermi energy level between the X and M points, in accordance with the occupation findings summarized in Fig. 3. However, these occupation differences do not directly explain the band splittings observed above the Fermi energy. Nonetheless, the changes in electronic structure evident from comparing the band structures suggest additional material properties may be affected because of the structural distortion. A detailed analysis of these effects is outside the scope of this work.

B. Monolayer

Beyond our investigation of bulk CuS_2, we extend our work to include its monolayer, which is formed as a quasilayered hexagonal structure along the close-packed (111) plane as illustrated in Fig. 5(b). We predict a stable phonon dispersion for this structure, as shown in Fig. 5(a). Neither a Kohn anomaly nor soft phonon modes are observed for the same electronic temperature range, indicating the absence of CDW order in the monolayer limit. This finding agrees with experimental results which saw no CDW signature in thin-film CuS_2 on a $SrTiO_3$ substrate [30].

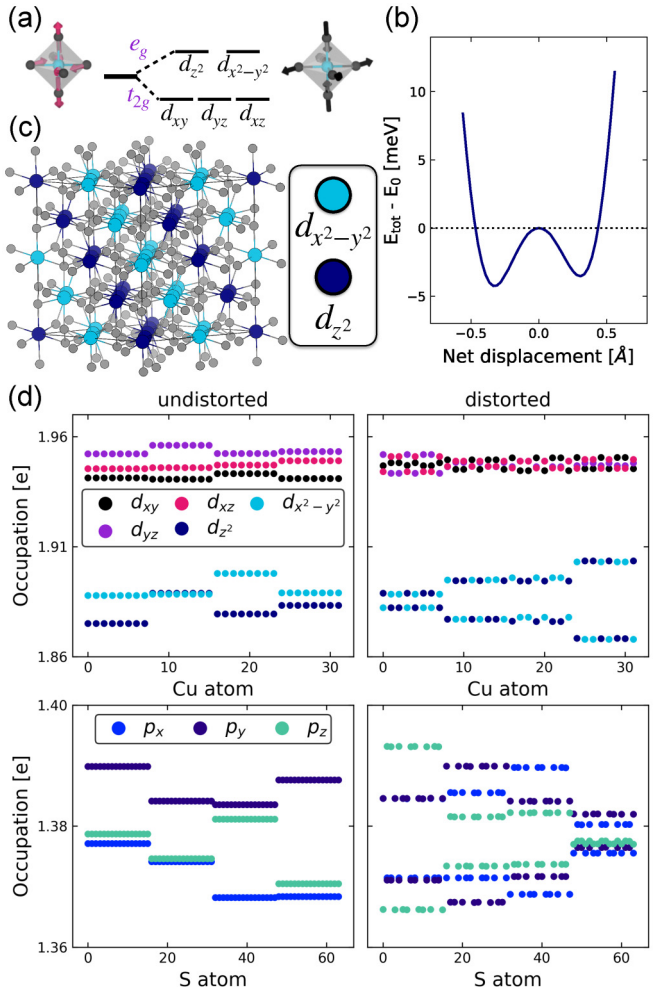

FIG. 3. Crystal field splitting and orbital occupation reordering. (a) Energy-level diagram for the octahedral configuration found in CuS_2 where the copper atom sits at the center and is surrounded by sulfur atoms. Also shown are the expansion and compression modes found for alternating octahedral sites [see Fig. 2(d)]. Of particular importance is that the constituents of the e_g and t_{2g} orbitals are energetically degenerate. (b) Potential energy surface computed for the $2 \times 2 \times 2$ supercell connecting the high- and low-symmetry structures via the effective phonon mode displacements, comprised of alternating octahedral expansions and compressions. The low-symmetry structure is roughly 4 meV lower in energy than the high-symmetry structure. (c) The distorted structure is shown with the copper atoms highlighted according to which e_g orbital is more occupied: $d_{x^2-y^2}$ or d_{z^2}. In the distorted structure, an alternating "row" of copper atoms prefers one of these orbitals. (d) Occupation of each of the copper d and sulfur p orbitals for each copper and sulfur atom within the $2 \times 2 \times 2$ supercell of CuS_2. The left shows the occupations for the undistorted structure, while the right shows the occupations in the distorted, lower-symmetry configuration. The x axis is arbitrary in ordering the atoms; however, the left and right panels have the same order. In general the effect of the distortion on these occupations is to allow for more diverse orbital occupation preferences for the different atomic sites in the crystal. (c) This is shown explicitly for the copper e_g orbitals; however, this can also be seen for the sulfur p and the copper t_{2g} orbitals. In the language of Jahn-Teller the broken symmetry removes the orbital degeneracies and brings the system, in this case the crystal, to an overall lower energy state.

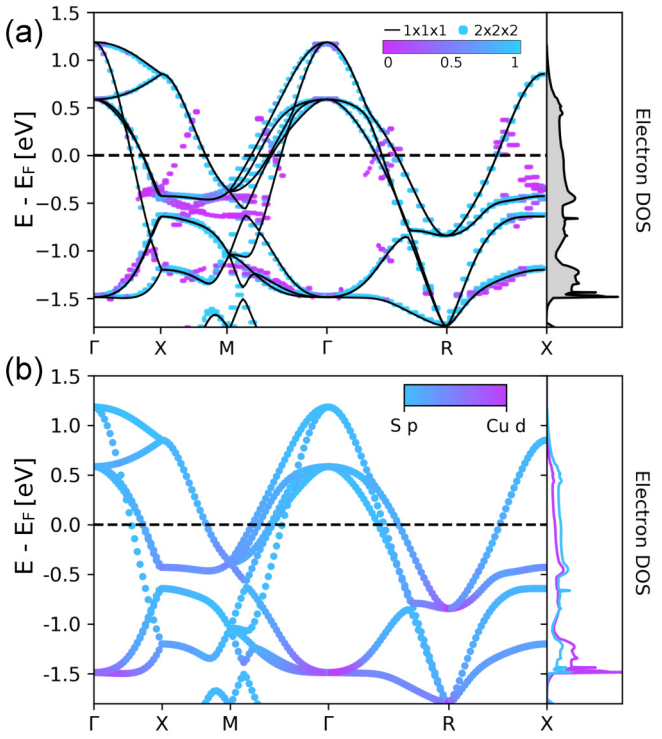

FIG. 4. Band splittings and electronic character. (a) Comparison of the unfolded band structure of the distorted phase ($2 \times 2 \times 2$) with that of the undistorted phase ($1 \times 1 \times 1$) superimposed as black lines. The supercell band structure is calculated via band unfolding [50], with the color of the points indicating the associated spectral weight (see color bar for reference). Also presented is the electronic density of states, which is not visibly distinguishable between the distorted and undistorted structures. (b) The orbital decomposed band structure, which is plotted as a function of relative sulfur p orbitals to copper d orbital. The density of states included corresponds to the relative density of states of these sets of atomic orbitals in the $1 \times 1 \times 1$ undistorted CuS_2 cell. The electronic character is in general more sulfur p than Cu d in character. See text for details.

This prediction raises questions as to why CDW order in bulk does not persist to the monolayer, in contrast to other layered TMDC materials [24,54,57,58]. Understanding the difference between these two structures opens up a new avenue to understand CDW formation in the bulk structure. We note that the monolayer cannot capture the sideways S_2 dimer motions seen in our calculated bulk distorted superstructure, and as a result, we find the stability of the monolayer is consistent with our predicted origin of the CDW behavior in bulk CuS_2. As noted earlier, we emphasize that many other CDW materials which exhibit CDW down to the monolayer tend to exist as layered, van der Waals systems, with large lattice spacings along the c axis. This means out-of-plane interactions tend to be weaker than in plane, and monolayers are formed by isolating just single layers of the bulk crystal. In the case of CuS_2, the monolayer belongs to a different symmetry configuration as it is extracted from the (111) direction of the bulk. It is therefore understandable that the role of dimensionality in CuS_2 may affect material properties differently than in other TMDCs.

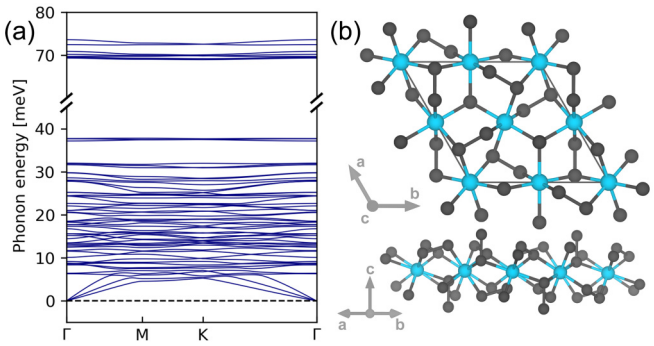

FIG. 5. Structural stability of monolayer CuS_2. (a) The predicted phonon dispersion of the monolayer structure shows no soft modes regardless of electronic temperature. (b) A top-down and side perspective of the lattice structure, equivalent to the (111) close-packed plane cut from the original bulk cubic structure. The phonon results indicate an absence of CDW in the monolayer, in accordance with recent experimental observations [30]. This absence is consistent with the results of Fig. 2, as the sideways S_2 motions could not be equivalently realized in the 2D limit.

IV. CONCLUSION

While the structural phase diagram of CuS_2 has remained a debate for years, we uncover critical information regarding its ability to manifest a CDW structure through theoretical and computational methods. We predict electronic-temperature-sensitive soft phonon modes that appear at low electronic temperatures in the experimentally reported structure of CuS_2, corresponding to a Kohn anomaly at the R point for an electronic temperature of approximately 100 K. We then realize the existence of a stable distorted phase with a $2a$ periodic lattice distortion and corresponding charge modulation at low electronic temperature. From this theoretical calculation, we establish a potential CDW transition and predict a crossover between the low- and high-symmetry structures at approximately 150 K, in impressive agreement with what is reported in experiment. We find this structural transition corresponds to periodic occupation changes in the Cu d and sulfur p orbitals around each Cu-centered octahedra, indicative of electron-phonon coupling. Finally, we predict a stable monolayer with no CDW order signatures observed, in agreement with recent experiments, and note the potential difference in available dimer distortions as a possible reason for the lack of CDW in the monolayer. One interesting direction for future work is the exploration of the dynamical stability of CuS_2.

Through this investigation of the phonon properties and electronic character of CuS_2, we report strong evidence of CDW in bulk CuS_2 and suggest Jahn-Teller-like behavior as an explanation for its occurrence. We also find that CuS_2 is similar to other TMDCs which exhibit low T_c superconductivity and CDW in the bulk, but unlike previously studied TMDCs, it does not exhibit CDW formation in its monolayer phase. As CDW formation is sometimes considered to suppress superconductivity, this difference between two and three dimensions indicates a unique opportunity to study the competition these two phenomena. Therefore, our findings also establish this material as an ideal system to study the interplay of CDW and superconductivity through comparison of its bulk and monolayer limits.

ACKNOWLEDGMENTS

The authors acknowledge funding from the Defense Advanced Research Projects Agency (DARPA) Defense Sciences Office (DSO) Driven and Nonequilibrium Quantum Systems program and the ONR grant on High-Tc Superconductivity at Oxide-Chalcogenide Interfaces (Grant No. N00014-18-1-2691). This research used resources of the National Energy Research Scientific Computing Center, a DOE Office of Science User Facility supported by the Office of Science of the U S Department of Energy under Contract No. DE-AC02-05CH11231, as well as resources at the Research Computing Group at Harvard University. J.C. recognizes the support of the DOE Computational Science Graduate Fellowship (CSGF) under Grant No. DE-FG02-97ER25308.

[1] A. H. Castro Neto, Phys. Rev. Lett. **86**, 4382 (2001).
[2] K. Rossnagel, J. Phys.: Condens. Matter **23**, 213001 (2011).
[3] P. Cudazzo, M. Gatti, and A. Rubio, Phys. Rev. B **86**, 075121 (2012).
[4] A. J. Frenzel, A. S. McLeod, D. Z.-R. Wang, Y. Liu, W. Lu, G. Ni, A. W. Tsen, Y. Sun, A. N. Pasupathy, and D. N. Basov, Phys. Rev. B **97**, 035111 (2018).
[5] D. N. Basov, R. D. Averitt, and D. Hsieh, Nat. Mater. **16**, 1077 (2017).
[6] B. Keimer and J. Moore, Nat. Phys. **13**, 1045 (2017).
[7] K. Cho, M. Kończykowski, S. Teknowijoyo, M. A. Tanatar, J. Guss, P. B. Gartin, J. M. Wilde, A. Kreyssig, R. J. McQueeney, A. I. Goldman, V. Mishra, P. J. Hirschfeld, and R. Prozorov, Nat. Commun. **9**, 2796 (2018).
[8] P. Chen, Y.-H. Chan, X.-Y. Fang, Y. Zhang, M. Y. Chou, S.-K. Mo, Z. Hussain, A.-V. Fedorov, and T.-C. Chiang, Nat. Commun. **6**, 8943 (2015).
[9] J. Chang, E. Blackburn, A. T. Holmes, N. B. Christensen, J. Larsen, J. Mesot, R. Liang, D. A. Bonn, W. N. Hardy, A. Watenphul, M. v. Zimmermann, E. M. Forgan, and S. M. Hayden, Nat. Phys. **8**, 871 (2012).
[10] R. F. Frindt, Phys. Rev. Lett. **28**, 299 (1972).
[11] Y. Yang, S. Fang, V. Fatemi, J. Ruhman, E. Navarro-Moratalla, K. Watanabe, T. Taniguchi, E. Kaxiras, and P. Jarillo-Herrero, Phys. Rev. B **98**, 035203 (2018).
[12] M. J. Wei, W. J. Lu, R. C. Xiao, H. Y. Lv, P. Tong, W. H. Song, and Y. P. Sun, Phys. Rev. B **96**, 165404 (2017).
[13] E. Navarro-Moratalla, J. O. Island, S. Mañas-Valero, E. Pinilla-Cienfuegos, A. Castellanos-Gomez, J. Quereda, G. Rubio-Bollinger, L. Chirolli, J. A. Silva-Guillén, N. Agraït *et al.*, Nat. Commun. **7**, 11043 (2016).
[14] X. Xi, L. Zhao, Z. Wang, H. Berger, L. Forró, J. Shan, and K. F. Mak, Nat. Nanotechnol. **10**, 765 (2015).

[15] L. Kang, B. Jin, X. Liu, X. Jia, J. Chen, Z. Ji, W. Xu, P. Wu, S. Mi, A. Pimenov *et al.*, J. Appl. Phys. **109**, 033908 (2011).

[16] T. A. Bither, R. J. Bouchard, W. H. Cloud, P. C. Donohue, and W. J. Siemons, Inorg. Chem. **7**, 2208 (1968).

[17] G. Krill, P. Panissod, M. F. Lapierre, F. Gautier, C. Robert, and M. N. Eddine, J. Phys. C **9**, 1521 (1976).

[18] H. Ueda, M. Nohara, K. Kitazawa, H. Takagi, A. Fugimori, T. Mizokawa, and T. Yagi, Phys. Rev. B **65**, 155104 (2002).

[19] F. Gautier, G. Krill, P. Panissod, and C. Robert, J. Phys. C **7**, L170 (1974).

[20] M. Kontani, T. Tutui, T. Moriwaka, and T. Mizukoshi, Phys. B: Condens. Matter **284-288**, 675 (2000).

[21] D. W. Bullett, J. Phys. C **15**, 6163 (1982).

[22] W. Temmerman, P. Durham, and D. Vaughan, Phys. Chem. Miner. **20**, 248 (1993).

[23] M. Kakihana, T. D. Matsuda, R. Higashinaka, Y. Aoki, A. Nakamura, D. Aoki, H. Harima, M. Hedo, T. Nakama, and Y. Ōnuki, J. Phys. Soc. Jpn. **88**, 014702 (2018).

[24] M. Calandra, I. I. Mazin, and F. Mauri, Phys. Rev. B **80**, 241108(R) (2009).

[25] D. L. Duong, M. Burghard, and J. C. Schön, Phys. Rev. B **92**, 245131 (2015).

[26] R. Bianco, M. Calandra, and F. Mauri, Phys. Rev. B **92**, 094107 (2015).

[27] J.-A. Yan, M. A. D. Cruz, B. Cook, and K. Varga, Sci. Rep. **5**, 16646 (2015).

[28] A. M. Brown, R. Sundararaman, P. Narang, W. A. Goddard, and H. A. Atwater, Phys. Rev. B **94**, 075120 (2016).

[29] S. N. Shirodkar, M. Mattheakis, P. Cazeaux, P. Narang, M. Soljačić, and E. Kaxiras, Phys. Rev. B **97**, 195435 (2018).

[30] C. Liu, H. Yang, C.-L. Song, W. Li, K. He, X.-C. Ma, L. Wang, and Q.-K. Xue, Chin. Phys. Lett. **35**, 027303 (2018).

[31] R. Peierls, Ann. Phys. **396**, 121 (1930).

[32] R. E. Peierls, *Quantum Theory of Solids* (Clarendon Press, Oxford, 1956).

[33] H. Fröhlich, Proc. R. Soc. London Ser. A **223**, 296 (1954).

[34] W. Kohn, Phys. Rev. Lett. **2**, 393 (1959).

[35] M. D. Johannes and I. I. Mazin, Phys. Rev. B **77**, 165135 (2008).

[36] M. Porer, U. Leierseder, J.-M. Ménard, H. Dachraoui, L. Mouchliadis, I. E. Perakis, U. Heinzmann, J. Demsar, K. Rossnagel, and R. Huber, Nat. Mater. **13**, 857 (2014).

[37] X. Zhu, Y. Cao, J. Zhang, E. W. Plummer, and J. Guo, Proc. Natl. Acad. Sci. U.S.A. **112**, 2367 (2015).

[38] R. Sundararaman, K. Letchworth-Weaver, K. A. Schwarz, D. Gunceler, O. Yalcin, and T. Arias, SoftwareX **6**, 278 (2017).

[39] C. J. Ciccarino, T. Christensen, R. Sundararaman, and P. Narang, Nano Lett. **18**, 5709 (2018).

[40] P. Narang, L. Zhao, S. Claybrook, and R. Sundararaman, Adv. Opt. Mater. **5**, 1600914 (2017).

[41] A. M. Brown, R. Sundararaman, P. Narang, W. A. Goddard, and H. A. Atwater, ACS Nano **10**, 957 (2016).

[42] R. Sundararaman, P. Narang, A. S. Jermyn, W. A. Goddard III, and H. A. Atwater, Nat. Commun. **5**, 5788 (2014).

[43] A. M. Rappe, K. M. Rabe, E. Kaxiras, and J. D. Joannopoulos, Phys. Rev. B **41**, 1227 (1990).

[44] A. Dal Corso, Comput. Mater. Sci. **95**, 337 (2014).

[45] J. P. Perdew, K. Burke, and M. Ernzerhof, Phys. Rev. Lett. **77**, 3865 (1996).

[46] M. Cococcioni and S. de Gironcoli, Phys. Rev. B **71**, 035105 (2005).

[47] See Supplemental Material at http://link.aps.org/supplemental/10.1103/PhysRevMaterials.4.104001 for additional information about the four instability-causing phonon modes, density-of-state changes for d orbitals, Hubbard U dependence, and the effects of different smearing types on the instability.

[48] N. Marzari, D. Vanderbilt, A. De Vita, and M. C. Payne, Phys. Rev. Lett. **82**, 3296 (1999).

[49] X. Tian, D. S. Kim, S. Yang, C. J. Ciccarino, Y. Gong, Y. Yang, Y. Yang, B. Duschatko, Y. Yuan, P. M. Ajayan, J. C. Idrobo, P. Narang, and J. Miao, Nat. Mater. **19**, 867 (2020).

[50] P. V. C. Medeiros, S. Stafström, and J. Björk, Phys. Rev. B **89**, 041407(R) (2014).

[51] G. Vanderschaeve and B. Escaig, Mater. Res. Bull. **11**, 483 (1976).

[52] H. Park, A. J. Millis, and C. A. Marianetti, Phys. Rev. Lett. **109**, 156402 (2012).

[53] S. Yi, Z. Zhu, X. Cai, Y. Jia, and J.-H. Cho, Inorg. Chem. **57**, 5083 (2018).

[54] B. Singh, C.-H. Hsu, W.-F. Tsai, V. M. Pereira, and H. Lin, Phys. Rev. B **95**, 245136 (2017).

[55] S. Sachdev and A. Georges, Phys. Rev. B **52**, 9520 (1995).

[56] S. Johnston, A. Mukherjee, I. Elfimov, M. Berciu, and G. A. Sawatzky, Phys. Rev. Lett. **112**, 106404 (2014).

[57] H. Ryu, Y. Chen, H. Kim, H.-Z. Tsai, S. Tang, J. Jiang, F. Liou, S. Kahn, C. Jia, A. A. Omrani, J. H. Shim, Z. Hussain, Z.-X. Shen, K. Kim, B. I. Min, C. Hwang, M. F. Crommie, and S.-K. Mo, Nano Lett. **18**, 689 (2018).

[58] D. Sakabe, Z. Liu, K. Suenaga, K. Nakatsugawa, and S. Tanda, npj Quantum Mater. **2**, 22 (2017).